Hindawi
Journal of Mathematics
Volume 2024, Article ID 1666959, 17 pages
https://doi.org/10.1155/2024/1666959

Research Article

Thermal Analysis of a Casson Boundary Layer Flow over a Penetrable Stretching Porous Wedge

Dur-e-Shehwar Sagheer,[1] Mohammad Alqudah,[2] Nawal A. Alshehri,[3] M. Sabeel Khan,[1] M. Asif Memon,[4] R. Shehzad,[1] and Amsalu Fenta[5]

[1]*Department of Mathematics, Capital University of Science and Technology, Islamabad 44000, Pakistan*
[2]*Department of Basic Sciences, School of Electrical Engineering & Information Technology, German Jordanian University, Amman 11180, Jordan*
[3]*Department of Mathematics and Statistics, College of Science, Taif University, P.O. Box 11099, Taif 21944, Saudi Arabia*
[4]*Department of Mathematics and Social Sciences, Sukkur IBA University, Sukkur 65200, Sindh, Pakistan*
[5]*Department of Physics, Mizan Tepi University, P.O. Box 121, Tepi, Ethiopia*

Correspondence should be addressed to Amsalu Fenta; amsalu.fenta09@gmail.com

Received 8 September 2023; Revised 16 January 2024; Accepted 7 March 2024; Published 18 March 2024

Academic Editor: M. M. Bhatti

This work aims to analyze the Casson thermal boundary layer flow over an expanding wedge in a porous medium with convective boundary conditions and ohmic heating. Moreover, the effects of porosity and viscous dissipation are studied in detail and included in the analysis. The importance of this study is due to its applications in biomedical engineering where the analysis of behavior of non-Newtonian blood flow in arteries and veins is desired. Within the context of blood flow, it is also applicable to many other fields, for instance, radiative therapy, MHD generators, soil machines, melt-spinning, and insulation processes. The modeled problem is a set of PDEs, which is nondimensionalized to derive a nonlinear boundary value problem (BVP). The obtained BVP is solved using the shooting technique, endowed with the order four Runge-Kutta and Newton methods. The impact of different parameters on the momentum and temperature fields is investigated along with two important parameters of physical significance, i.e., the Nusselt number and the surface drag force. Results are validated, and an excellent agreement is seen for the parameters of interest using MATLAB built-in function bvp4c. A significant finding is that by increasing the Casson liquid parameter, the velocity decreases as the wedge expands quicker than the free stream velocity at $R = 2$. However, the velocity increases for the case when $R = 0.1$. A decrease in the Darcy number increases the temperature profile. Furthermore, the convective parameter accelerated the heat transmission rate, and a rise in the Prandtl number thickens the thermal boundary layer. The findings of this investigation contribute to problems in fluid dynamics and heat transfer that involve studying the behavior of a non-Newtonian fluid with Casson rheological properties near a solid porous wedge surface.

1. Introduction

Mixed convection across an impermeable or permeable wedge is used in many manufacturing processes, including extruding molten polymers, fabricating plastic sheets for solar energy, and storing thermal energy. According to Shah et al. [1], mixed convection is a fluid flow phenomenon characterized by the simultaneous effect of forced convection, which is caused by external forces such as a pump or a fan, and natural convection, which is caused by buoyant forces caused by temperature gradients within the fluid. Systems such as technical equipment and natural phenomena such as the movement of temperature stratified masses of air and water on Earth exhibit mixed convection flow [2, 3]. It has uses in heat exchangers [4], thermal design, cooling electronic components, and other fields. It is also pertinent to heat transfer and fluid flow analysis. Karwe and Jaluria [5, 6] explained that the investigation is necessary to check the quality of resulting products and cooling rates. Ishak et al. [2] investigated the mixed convection

magnetohydrodynamics boundary layer across a vertically expanding sheet while the wall temperature remained unchanged. The reader is referred to [1, 7, 8] for a good overview on the mixed convection MHD viscoelastic fluid flow analysis.

Some recent studies have also considered the mixed convective flow in analyzing the porous flow structures. In this connection, thermal analysis in a higher grade Forchheimer porous nanostructure bounded between nonisothermal plates is investigated by Saleem et al. [9]. They utilized a finite difference approach in their analysis. The transient problem of mixed convection over a vertically moving wedge was examined by Ravindran et al. [10]. Numerical results show that the buoyant force enhances the skin friction and Nusselt number. The thermal properties of magnetohydrodynamics of Falkner–Skan Casson flow sideways a moving wedge are analyzed by Ullah et al. [11]. They used finite difference and quasilinearization techniques to derive the problem's solution. It is detected that an augmentation in the values of the Eckert number has a negligible impact on force convection flow. They discovered that the existence of the suction or injection changes the rates of skin friction, concentration, and heat transfer. Unsteady flow with mixed convection dusty flow across a vertical wedge was investigated by Hossain et al. [3].

Many of the above-described studies addressed the flow convection over a vertical porous wedge. It is worth mentioning that there is limited research about convection flow in the presence of suction/injection, viscous and ohmic dissipation upon a permeable/impermeable wedge. The numerical solution of thermal radiation influence on magnetohydrodynamics with forced convective flow adjacent to a wedge with a heat source/sink [12] was computed by Chamkha et al. [13] employing the implicit finite difference technique. Anwar Hossain et al. [14] have explored the problem of MHD flow via a wedge with variable surface temperature. Additionally, perturbation solutions for different values of τ dimensions of time are discovered. Su et al. [15] investigated the MHD mixed convective flow of heat transfer across a permeable stretched wedge using numerical and analytic (DTM) methods. Also, the authors demonstrated that as the domain becomes unbounded, the DTM-BF solutions diverge. The influence of chemical reaction on the mixed convection magnetohydrodynamics and heat transfer across a porous wedge was investigated by Kandasamy et al. [16]. This research concludes that in a mixed convective regime, there is an increase in the hydrodynamic layer. In contrast, the concentration and temperature boundary layers decrease by lowering the values of the suction parameter. The issue of MHD flow through a porous nonisothermal wedge was examined by Prasad et al. [17]. They observed that among all variables, the mixed convection parameter substantially impacts the surface drag force, thermal rate, normal velocity of the wall, and temperature profile of the MHD flow through a porous nonisothermal wedge. Transient Falkner–Skan liquid flow of Carreau microliquid via a still/moving wedge was demonstrated by Khan et al. [18].

Due to the numerous applications in radiative therapy, metal casting technology, and ceramic engineering, several studies [4, 19] have explored the influence of radiative effect at the boundary layer with the transfer of heat characteristics. In biomedical engineering, within the context of blood flow [20, 21], the Casson parameter has been considered in analyzing the behavior of non-Newtonian flow in arteries [22–24]. For a detailed review of the use and applications of Casson nanofluid flow, the reader is also referred to the work of Nayak et al. [25] who have investigated the Casson nanofluid flow subjected to biomedicine applications and chemical reactions [26–28]. For some other important applications related to heat transfer enhancement, the reader is referred to the work of [29] and references therein. Ullah et al. [30] have investigated the Casson liquid flow across a nonstationary wedge using the effect of thermophoresis and Brownian diffusion. The transportation of heat for homogeneous/heterogeneous Casson liquid in a porous medium was studied by Bilal et al. [31]. The velocity, temperature, and concentration of solutions for homogeneous and heterogeneous reactions are fundamental limitations of the basic subsidized flow parameters. Several researchers investigated the impact of heat radiation on different flow problems [32–34] using finite element strategies.

Viscous dissipation can significantly affect the temperature distribution and overall energy balance of the system. Similarly, porous media have a large contact surface with fluids, which can significantly increase the heat transfer effect. The porous medium changes the flow field conditions, and the conduction heat transfer coefficient is usually higher than that of the fluid studied. The main aim of this study is to extend the work of Hussain et al. [35] by considering the following additional physical effects:

(i) The Casson thermal boundary layer flow rheology is assumed

(ii) The effects of porosity and viscous dissipation are taken into account

In this respect, two important parameters of physical interest arises are the viscous dissipation parameter E_c and the porosity parameter D_a. The specific goals and objectives of the study are to investigate the following research questions:

(i) How does a porous wedge flow's thermal reaction to Casson flow rheology behave?

(ii) How does the porosity affect the velocity and thermal profiles in the presence of Casson rheology?

(iii) How does the viscous dissipation affect the hydrodynamic profiles of the present rheology?

(iv) How do the viscous dissipation and porosity of the Casson fluid affect the skin-friction coefficient and Nusselt number?

The next section presents the modeling aspects of the modeled problem which is first transformed to a boundary value problem in ordinary differential equations. The problem is then solved numerically by the shooting method, and obtained results are discussed.

2. Mathematical Modeling

This problem considers an electrically conducting thermal radiative 2D Casson fluid flow with mixed convection on a moving wedge as shown in Figure 1. The conservation equations for mass, momentum, and energy for viscous incompressible fluid in the presence of the viscous dissipation, Rosseland radiation, and porosity constitute the modeling description of the considered flow and are described respectively as [36]

$$\nabla \cdot V = 0, \tag{1}$$

$$\rho (V \cdot \nabla) V = \nabla \cdot \mathbf{S} - \frac{\mu}{K} V + \rho g, \tag{2}$$

and

$$\rho C_p (V \cdot \nabla) T = \alpha \nabla^2 T + \alpha \left[\left(\frac{\partial u}{\partial x} \right)^2 + \left(\frac{\partial v}{\partial y} \right)^2 \right] - \frac{\partial}{\partial y} (q_r) + \frac{\nu_f}{C_p} \left(\frac{du}{dy} \right)^2. \tag{3}$$

where in equation (2), the symbol $\mathbf{S}$ represents the stress tensor of the considered fluid, which is represented by

$$\mathbf{S} = -\nabla p + \boldsymbol{\tau} - \sigma B^2 V. \tag{4}$$

The rheological equation for the incompressible flow of the Casson fluid is given by [37]

$$\tau_{\mathrm{ij}} = \begin{cases} 2\left(\mu + \dfrac{p_y}{\sqrt{2\pi}} \right) e_{\mathrm{ij}}, & \pi > \pi_c, \\ 2\left(\mu + \dfrac{p_y}{\sqrt{2\pi_c}} \right) e_{\mathrm{ij}}, & \pi < \pi_c, \end{cases} \tag{5}$$

where e_{ij} are the components of the strain tensor defined as

$$\mathbf{e} = \frac{1}{2} \left(\nabla V + \nabla V^T \right). \tag{6}$$

In equation (5), π is the product of the component of the deformation rate with itself, $\pi = e_{\mathrm{ij}} e_{\mathrm{ij}}$, π_c is a critical value of this product based on the non-Newtonian model, and p_y is the yield stress of the fluid. The Cartesian coordinates' system is denoted by (x, y) from which x-direction is along the wedge and y-direction is normal. The velocity of the wedge is represented by U_w, and the velocity that is distant from the wedge is U, which depends on x, i.e., $U = U_0 x^m$. The stretching wedge has suction and injection velocity, denoted by v_w. During the heating of the wedge, a hot fluid with temperature T_f produces a high heat transfer coefficient h_f, where T_∞ is the temperature of the fluid away from the wedge. The uniform magnetic field is denoted by B, acting along y-direction and equivalent to $B = B_o x^{m-1/2}$. The wedge angle is denoted by $\Omega = \beta\pi$.

2.1. Dimensional Equations. Connected flow equations with boundary conditions are (see for reference [15])

$$u_x + v_y = 0, \tag{7}$$

$$\begin{aligned} u u_x + v u_y = U \frac{dU}{dx} + \nu \left(1 + \frac{1}{\delta} \right) u_{\mathrm{yy}} + g \beta_o (T - T_\infty) \sin \frac{\Omega}{2} - \frac{\sigma B^2}{\rho} (u - U) \\ - \frac{\nu \Phi u}{k} - \frac{C_b \Phi u^2}{\sqrt{k}}, \end{aligned} \tag{8}$$

$$\rho c_p \left(u T_x + v T_y \right) = -u \left(\rho U \frac{dU}{dx} + \sigma B^2 U \right) + \alpha T_{\mathrm{yy}} - (q_r)_y + \sigma B^2 u^2 + \left(1 + \frac{1}{\delta} \right) \frac{\mu}{\rho c_p} \left(u_y \right)^2. \tag{9}$$

The boundary conditions are described as follows:

$$u|_{(x,0)} = \mathrm{RU}, \tag{10}$$

$$v|_{(x,0)} = v_w = -(\nu U_o)^{1/2} C \left(\frac{m+1}{2} \right) x^{m+1/2}, \tag{11}$$

$$T_y|_{(x,0)} = \frac{h}{k} \left(T - T_f \right), \tag{12}$$

$$u|_{(x,\infty_n)} \longrightarrow U_o x^m, T|_{(x,\infty_n)} \longrightarrow T_{\infty_n}. \tag{13}$$

For the physical description of these boundary conditions, the reader is referred to the work of Su et al. [15]. Here, ν, g, β_o, σ, ρ, c_p, and α denote the kinematic viscosity, gravity field, coefficient of thermal expansion, conductivity of fluid due to electric current, fluid density, heat capacity, and thermal conductivity, respectively. The term $\partial q_r / \partial y$ here q_r is radiative heat flux and is equal to $-4\sigma_o / 3k^* \partial T^4 / \partial y$, where

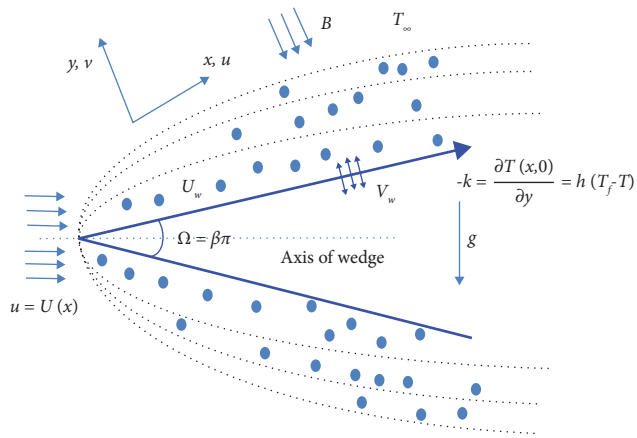

Figure 1: Geometry of the problem.

σ_o and k^* are known as the Stefan–Boltzman parameter and mean absorption coefficient, respectively. $\beta = \mu_B\sqrt{2\pi_c}/p_y$ is the parameter of Casson fluid.

2.2. Similarity Transformations. Here, in this subsection, the similar similarity transformations are introduced. Similar transformations are employed [15] to simplify the set of governing equations of a complex physical problem by converting them dimensionless and making them similar in structure.

$$\begin{aligned} \psi &= \sqrt{U\nu x}\, f, \\ u &= \frac{\partial \psi}{\partial y}, \\ v &= -\frac{\partial \psi}{\partial x}, \\ \eta &= \sqrt{\frac{U_o}{\nu}}\, x^{m-1/2} y, \\ \theta(\eta) &= \frac{T - T_\infty}{T_f - T_\infty}. \end{aligned} \tag{14}$$

These are particularly useful for analyzing the flow and heat transfer phenomenon scales with changing parameters like Reynolds and Nusselt numbers. There are a lot of situations when one needs to introduce nonsimilar transformations [38] to convert this physical system into a nondimensional form. Such situations arise when nonstandard boundary conditions [39–41] are introduced in the mathematical description of the flow problems.

2.3. Nondimensional Equations. Equations (8)–(13) are nondimensionalized using transformations in Section 2.2. The resulting equations take the form:

$$\begin{aligned} f''' = \left(\frac{\delta}{1+\delta}\right)\Big[&-\frac{m+1}{2} ff'' - (m+M) + (m+\alpha_1) f'^2 + (M + (\mathrm{Da})^{-1}) f' \\ &-\lambda \sin\frac{\Omega}{2}\theta\Big], \end{aligned} \tag{15}$$

$$\begin{aligned} \theta'' = \frac{-1}{(1+\mathrm{Nr})}\Big[&\mathrm{Pr}\left(\frac{m+1}{2}\right) f\theta' - \mathrm{mEcPrf}' - \mathrm{MEcPrf}' + \mathrm{MEcPrf}'^2 \\ &+\left(1+\frac{1}{\delta}\right)\mathrm{PrEcf}''^2\Big], \end{aligned} \tag{16}$$

along with the dimensionless BCs as

$$\left.\begin{aligned}&\theta'(0) = -B_i + B_i\theta(0), \theta(\infty_n) = 0,\\ &f'(0) = R, f'(\infty_n) = 1, f(0) = C\end{aligned}\right\}. \tag{17}$$

2.4. Dimensionless Parameters. The associated dimensionless parameters are

$$M = \frac{\sigma B_o^2}{\rho U_o}, \lambda = \frac{\mathrm{Gr}_x}{\mathrm{Re}_x^2}, \mathrm{Gr}_x = \frac{g\beta_o\left(T_f - T_\infty\right)x^3}{\nu^2},$$

$$\mathrm{Re}_x = \frac{Ux}{\nu}, \mathrm{Nr} = \frac{16T_\infty^3\sigma_o}{3k^*\alpha}, \mathrm{Ec} = \frac{U^2}{c_p\left(T_f - T_\infty\right)},$$

$$\mathrm{Pr} = \frac{\mu c_p}{\alpha}, B_i = \frac{h}{k}\sqrt{\frac{\nu x}{U}}, \mathrm{Da}^{-1} = \frac{\nu\Phi}{kU_o x^{m-1}}, \alpha_1 = \frac{C_b\Phi x}{\sqrt{k}}. \tag{18}$$

3. Quantities of Interest

3.1. Surface Drag Force. The dimensional form of the skin friction is as follows:

$$C_f = \frac{\mu_\beta\left(1 + p_y/\mu_\beta\sqrt{2\pi}\right)\partial u/\partial y|_{y=0}}{\rho U^2}, \tag{19}$$

where μ_β represents the viscosity of the liquid and p_y is the liquid yield stress. The nondimensional form of surface drag force is given as

$$\left(\mathrm{Re}_x\right)^{1/2}C_f = \left(1 + \frac{1}{\delta}\right)f''(0). \tag{20}$$

3.2. Local Nusselt Number. The local Nusselt parameter is described as

$$\mathrm{Nu}_x = \frac{xq_w}{\alpha\left(T_f - T_\infty\right)}, \tag{21}$$

where q_w is the conductive heat flux from the surface of the wedge.

$$\left(\mathrm{Re}_x\right)^{-1/2}\mathrm{Nu}_x = -\theta'(0). \tag{22}$$

4. Solution Method through Shooting and bvp4c

The above nonlinear ODEs are now solved through the shooting method. This numerical technique is used for finding the solution to a boundary value problem. Using the following derivatives, the boundary value problem is transformed into a first-order initial value problem (see Table 1).

Using the above notations, equations (15) and (16) are transformed into the following fifteen ODEs:

$$y_1' = y_2; y_1(0) = C,$$

$$y_2' = y_3; y_2(0) = R,$$

$$y_3' = \frac{1}{(1 + 1/\delta)}\left[-\frac{m+1}{2}y_1y_3 - (m + M) + (m + \alpha_1)y_2^2 + \left(M + (\mathrm{Da})^{-1}\right)y_2 - \lambda\sin\frac{\Omega}{2}y_4\right],$$

$$y_3(0) = s,$$

$$y_4' = y_5; y_4(0) = q,$$

$$y_5' = \frac{-1}{(1 + \mathrm{Nr})}\left[\mathrm{Pr}\left(\frac{m+1}{2}\right)y_1y_5 - \mathrm{mEcPry}_2 - \mathrm{MEcPry}_2 + \mathrm{MEcPry}_2^2 + \left(1 + \frac{1}{\delta}\right)\mathrm{PrEcy}_3^2\right],$$

$$y_5(0) = -\mathrm{Bi}(1 - q),$$

$$y_6' = y_7; y_6(0) = 0,$$

$$y_7' = y_8; y_7(0) = 0,$$

Table 1: Denotation of unknown variables.

$f = y_1$ $f''' = y_3'$ $\theta'' = y_5'$	$f' = y_1' = y_2$ $\theta = y_4$	$f'' = y_2' = y_3$ $\theta' = y_4' = y_5$

$$
\begin{aligned}
y_8' &= \frac{1}{(1+1/\delta)}\left[-\frac{m+1}{2}\left(y_6y_3+y_1y_8\right)+2\left(m+\alpha_1\right)y_2y_7+\left(M+(\mathrm{Da})^{-1}\right)y_7\right.\\
&\quad\left.-\lambda\sin\frac{\Omega}{2}y_9\right],\\
y_8(0) &= 1,\\
y_9' &= y_{10};\, y_9(0) = 0,\\
y_{10}' &= \frac{-1}{(1+\mathrm{Nr})}\left[\mathrm{Pr}\left(\frac{m+1}{2}\right)\left(y_6y_5+y_1y_{10}\right)-\mathrm{mEcPry}_7-\mathrm{MEcPry}_7\right.\\
&\quad\left.+2\mathrm{MEcPry}_2y_7+2\left(1+\frac{1}{\delta}\right)\mathrm{PrEcy}_3y_8\right],\\
y_{10}(0) &= 0,\\
y_{11}' &= y_{12};\, y_{11}(0) = 0,\\
y_{12}' &= y_{13};\, y_{12}(0) = 0,\\
y_{13}' &= \frac{1}{(1+1/\delta)}\left[-\frac{m+1}{2}\left(y_{11}y_3+y_1y_{13}\right)+2\left(m+\alpha_1\right)y_2y_{12}+\left(M+\mathrm{Da}^{-1}\right)y_{12}\right.\\
&\quad\left.-\lambda\sin\frac{\Omega}{2}y_{14}\right],\\
y_{13}(0) &= 0,\\
y_{14}' &= y_{15};\, y_{14}(0) = 1,\\
y_{15}' &= \frac{1}{(1+\mathrm{Nr})}\left[-\mathrm{Pr}\left(\frac{m+1}{2}\right)\left(y_{11}y_5+y_1y_{15}\right)+\mathrm{mEcPry}_{12}\right.\\
&\quad\left.+\mathrm{MEcPry}_{12}-2\left(1+\frac{1}{\delta}\right)\mathrm{MEcPry}_2y_{12}\right],\\
y_{15}(0) &= B_i,
\end{aligned}
\tag{23}
$$

where s and q are the missing initial conditions. Choose the missing initial conditions that satisfy the above boundary conditions. The RK-4 method is applied to solve the first-order initial value problem. Newton's numerical technique is used to refine the starting values. This iteration is repeated until the values meet the required accuracy, achieved by getting sufficiently close to the given boundary conditions. The stopping criteria for Newton's method are given as follows:

$$\max\left(\left|\phi_1\left(\eta_\infty, s_n, q_n\right)\right|,\ \left|\phi_2\left(\eta_\infty, s_n, q_n\right)\right|\right) < \epsilon, \tag{24}$$

Here, $\epsilon = 10^{-8}$.

The solution of the above model boundary value problem can also be calculated through the built-in MATLAB function bvp4c. This built-in function is suitable for solving higher-order boundary value problems in fluid mechanics. The criteria behind the bvp4c function are the three-stage Lobatto III-a formula, implemented by the finite difference algorithm [42]. This formula uses collocation, and the collocation polynomial offers a C^1-continuous solution that is consistently fourth-order accurate across the integration interval of the problem. The residual of the continuous solution serves as the foundation for mesh selection and error control in the model problem. The integration interval is split into smaller intervals using the collocation technique and a mesh of points. The solver can arrive at a numerical solution by resolving a global system of algebraic equations caused by the boundary conditions and the collocation conditions placed on each subinterval. The solver then determines how much each subinterval's numerical solution error is. The solver adjusts the mesh and restarts the procedure if the solution does not meet the tolerance conditions. In addition to an initial approximation of the solution at the mesh points, one must supply the initial mesh points.

5. Analysis of Results

This research is focused on analyzing the following aspects:

(1) The steady nonlinear conducting radiative Casson flow through a penetrable wedge is examined with ohmic heating, thermal behavior, suction/injection, and convective BC.

Table 2: Results of $(\mathrm{Re}_x)^{1/2}C_f$ and $(\mathrm{Re}_x)^{-1/2}\mathrm{Nu}_x$ for values of β.

R	β	Shooting		bvp4c	
		C_f	Nu_x	C_f	Nu_x
0.3	0.0	1.69658760891	0.63337168742	1.69658760047	0.63337154600
2.0	0.0	−2.89008774386	0.45899909881	−2.89008775215	0.45899909775
0.3	0.7	2.07949724747	0.62651534840	2.07949724751	0.62651534840
2.0	0.7	−2.50129930834	0.45694769615	−2.50129931309	0.45694769229
0.3	1	2.13879844844	0.62521388870	2.13879844837	0.62521389153
2.0	1	−2.44050791207	0.45640487833	−2.44050791544	0.45640487686

(2) The effects of porosity and viscous dissipation are considered.

(3) Drag caused by the friction of a fluid against the surface and heat transfer due to pure conduction is examined by calculating the numerical values of the skin-friction coefficient and Nusselt number by varying the values of wedge angle β and the magnetic parameter M.

(4) Thickness of the momentum boundary layer is examined for magnetic parameter M, wedge range β, Casson parameter δ, Prandtl number P_r, and radiative heat transfer parameter N_r.

(5) Thermal boundary layer is analyzed through the numerical results by varying the Eckert number E_c, Biot number B_i, Darcy number D_a, Prandtl number P_r, and radiative heat transfer parameter N_r.

6. Results and Discussion

This section describes the outcomes of the model presented above through the discussed shooting technique. Table 2 shows the values of the heat rate parameter $|\theta'(0)|$ and drag force parameter $f''(0)$ for various values of the wedge angle β and velocity ratio parameter R. When R is less than or more than 1, surface drag force increases as the angle β increases. It is also seen that by an increase in β, the temperature gradient coefficient of Nusselt number $|\theta'(0)|$ decreases. The results acquired by the shooting approach are verified by BVP4C as well. Here, the values of different parameters are fixed as $\delta = 1$, $m = 0.1$, $\lambda = 0.8$, $B_i = 5$, $M = 0$, Nr = 1, Pr = 1, Ec = 0.5, $C = 1$, $(\mathrm{Da})^{-1} = 0.01$, and $\alpha_1 = 0.01$.

The numerical effects of drag force and Nusselt number for various values of the velocity ratio parameter R and the magnetic parameter M are shown in Table 3. The values of the Nusselt coefficient $\theta'(0)$, surface drag force coefficient $f''(0)$, and magnetic coefficient M rise when R is less than 1. When R is more than 1, the skin-friction coefficient and $|\theta'(0)|$ both drop as the magnetic coefficient M values increase. The outcomes obtained using the shooting approach are likewise met by bvp4c.

6.1. The Velocity Profiles. The impact of the Casson parameter δ on the velocity profile $f'(\eta)$ at $R = R/\{1\}$ is seen in Figure 2(a). Increases in δ steepen the velocity profile $f'(\eta)$ when R is less than one, whereas increases in δ deplete the velocity profile $f'(\eta)$ as $R = 2$. For the case $R < 1$, Figure 2(b) shows an inverse relationship between the velocity profile and the magnetic parameter M; however, for $R < 1$, the relationship is the reverse. The Lorentz force that the magnetic field produces is what causes this phenomenon. For both situations of R, Figure 2(c) shows an increase in velocity $f'(\eta)$ through an increase in the wedge's β angle. The velocity boundary layer thickens with an increase in the velocity ratio (R), as seen in Figure 3(a). The velocity boundary layer thickens with an increase in the velocity ratio (R), as seen in Figure 3. The effects of radiation parameter Nr and Prandtl number Pr on the velocity profile are shown by generating Figures 3(b) and 3(c) from the numerical results. The figures show that for both situations of R, there is a fall in the velocity profile due to cumulative values of the Prandtl number and decreasing values of the radiation parameter. Three key implications are shown in Figure 4. To demonstrate how the Biot number affects the velocity profile, Figure 4(a) is drawn. The ratio of the body's internal conductive resistance to its surface-measured external convective resistance is known as the convection parameter Bi. It is observed that temperature is improved when internal conductive resistance is increased rather than exterior convective resistance and thus raises the velocity profile $f'(\eta)$. Figure 4(b) illustrates how Eckert number Ec has a major influence. This figure shows that for $R < 1$, $f'(\eta)$ is a decreasing function of Ec; however, the behavior is reversed when $R = 2$. As can be seen in Figure 4(c), the depth of the momentum barrier layer decreases as the Darcy parameter Da decreases.

6.2. The Temperature Profile. The influence of the Casson coefficient δ on the temperature profile $\theta(\eta)$, at $R = 0.1$ and $R = 1.5$, is shown in Figures 5(a) and 6. The temperature profile decreases in all scenarios when δ increases. Figure 5(b) illustrates how changing the magnetic parameter M affects the momentum boundary layer's behavior. The graph indicates that $\theta(\eta)$ decreases for rising values of M for $R = 0.3$ and exhibits opposite behavior at $R = 2$. A direct relationship between the wedge angle β and the temperature profile is seen in Figure 5(c). Three important effects on thermal profiles are depicted in Figure 7. Here, Figure 6(a) demonstrates how the thickness of the thermal boundary layer decreases as the radiation parameter Nr decreases. The thermal profile $\theta(\eta)$ decreases as the Prandtl number accumulates, as seen in Figure 6(b). The temperature profile $\theta(\eta)$ decreases as the velocity ratio parameter R increases, as

Table 3: Results of $(\mathrm{Re}_x)^{1/2}C_f$ and $(\mathrm{Re}_x)^{-1/2}Nu_x$ for values of M.

R	M	Shooting		bvp4c	
		C_f	Nu_x	C_f	Nu_x
0.3	0.0	1.20318792005	0.54890507691	1.20318792186	0.49094985376
0.3	1.0	1.76577658883	0.63233066638	1.76577658484	0.63233066766
0.3	1.5	1.98524900184	0.66398690612	1.98524900046	0.66398690879
2.0	0.0	−2.19942925344	0.73146211947	−2.19942925346	0.73146211939
2.0	4.0	−4.17193636185	−0.10738670687	−4.17193636668	−0.10738670215
2.0	4.5	−4.35643483323	−0.18263653574	−4.35643483570	−0.18263653376

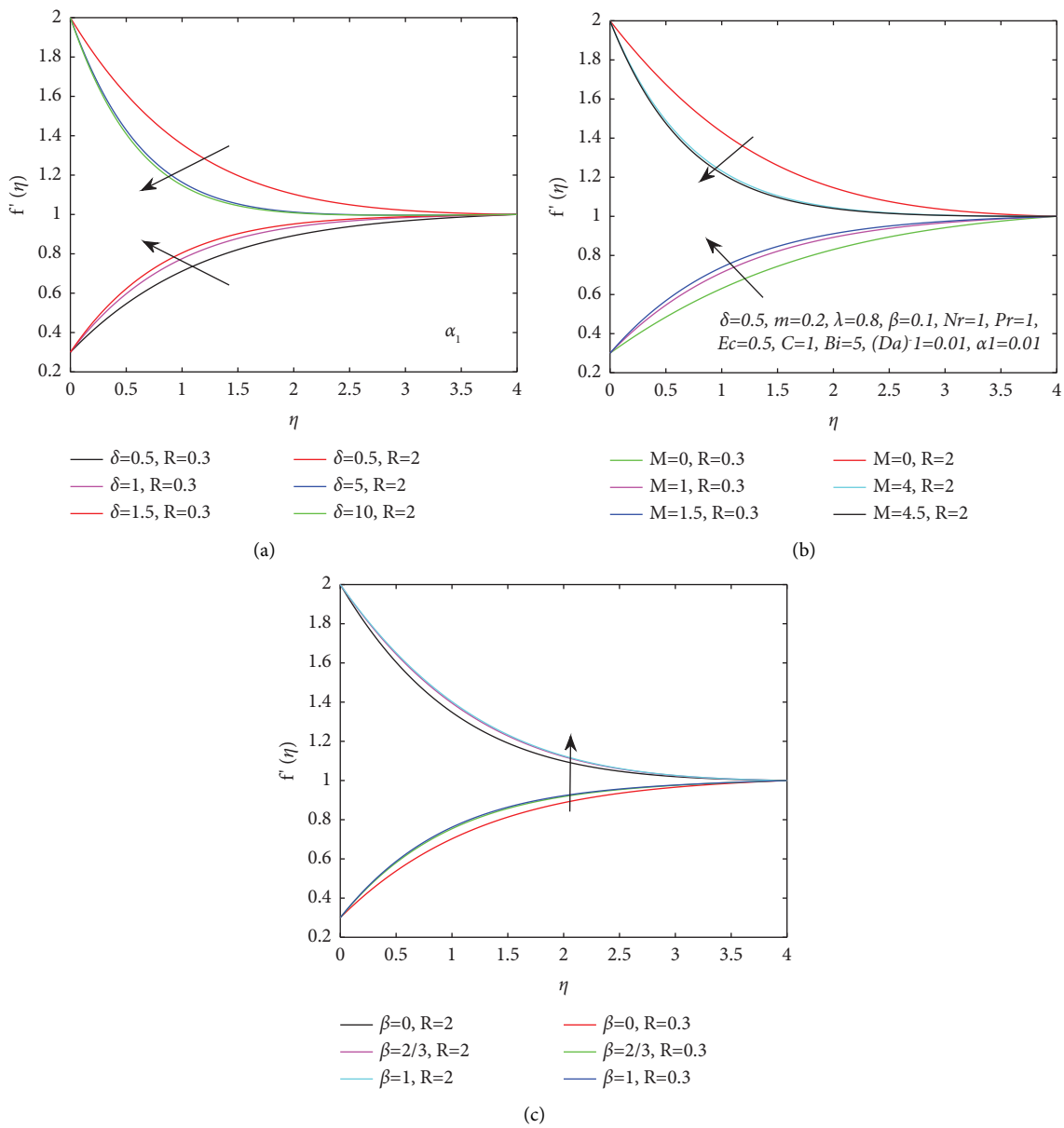

Figure 2: Effects of the magnetic parameter M, Casson parameter δ, and wedge angle β on the velocity profile. (a) $f'(\eta)$ for various values of δ. (b) $f'(\eta)$ for various values of M. (c) $f'(\eta)$ for various values of β.

seen in Figure 6(c). The temperature's relationship with the Eckert number is seen in Figure 8(a). When Ec rises, the temperature profile decreases. The effect of convective number Bi is seen in Figure 8(b). Increasing Bi levels increases the body's internal conductive resistance. The behavior of temperature $\theta(\eta)$ is steepened. Figure 8(c)

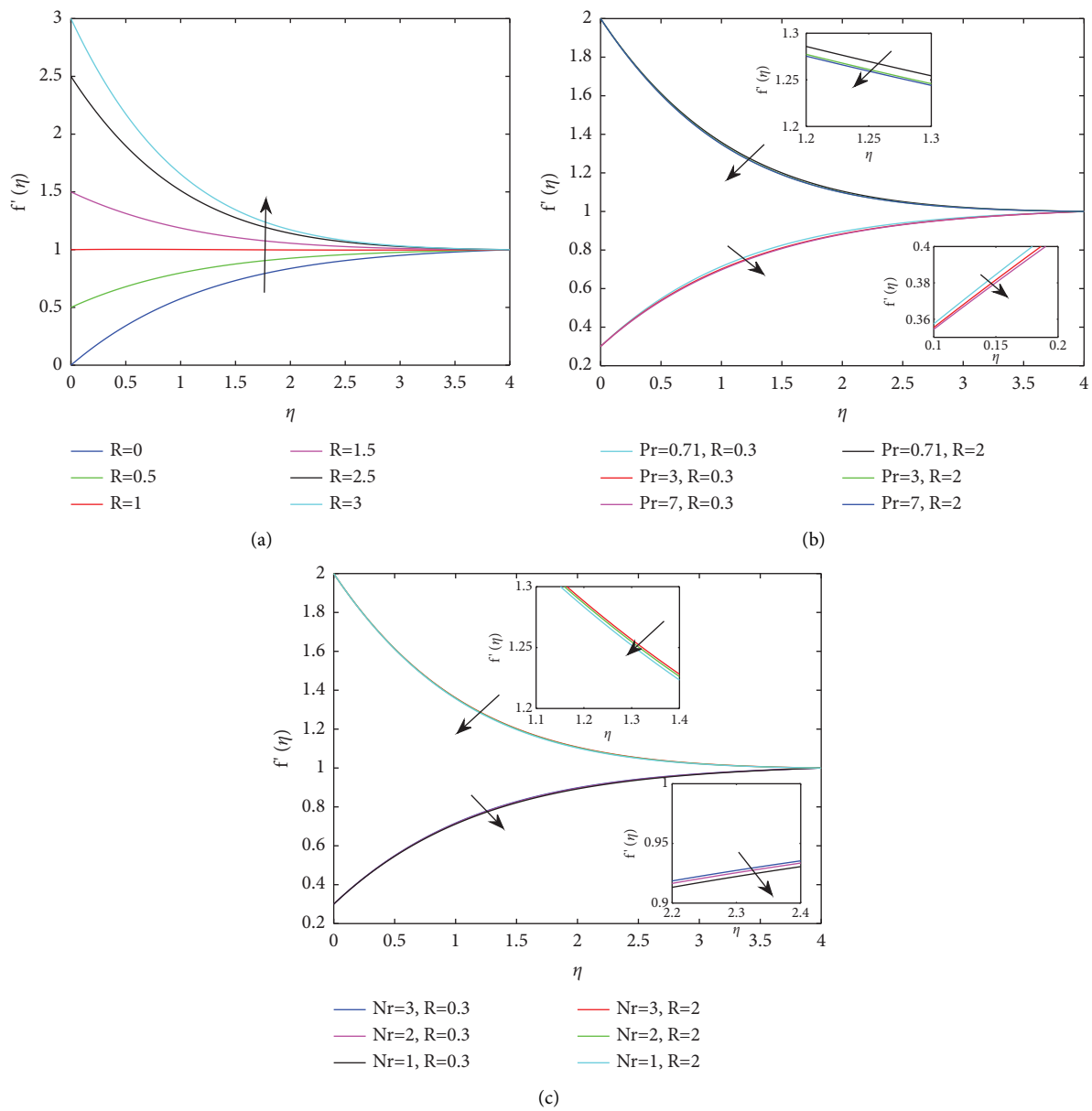

Figure 3: Impacts of the velocity ratio parameter R, Prandtl number Pr, and radiative heat transfer parameter Nr on the velocity profile. (a) Effects of R on $f'(\eta)$. (b) Effects of Pr on $f'(\eta)$. (c) Influence of Nr on $f'(\eta)$.

illustrates how $\theta(\eta)$ increases along with a drop in the Darcy number Da. The following fixed values apply to the selection of various parameters: $\delta = 1, m = 0.2, \lambda = 0.8, B_i = 5, M = 0$, $\mathrm{Nr} = 1, \mathrm{Pr} = 1, \mathrm{Ec} = 0.5, C = 1$, $(\mathrm{Da})^{-1} = 0.01$, and $\alpha_1 = 0.01$

6.3. Nusselt Number and Surface Drag Force Coefficient. The relationship between the Nusselt number and Pr and Bi is evident in Figure 7(a). On the other hand, Figure 7(b) shows that skin friction rises with increasing Bi values but

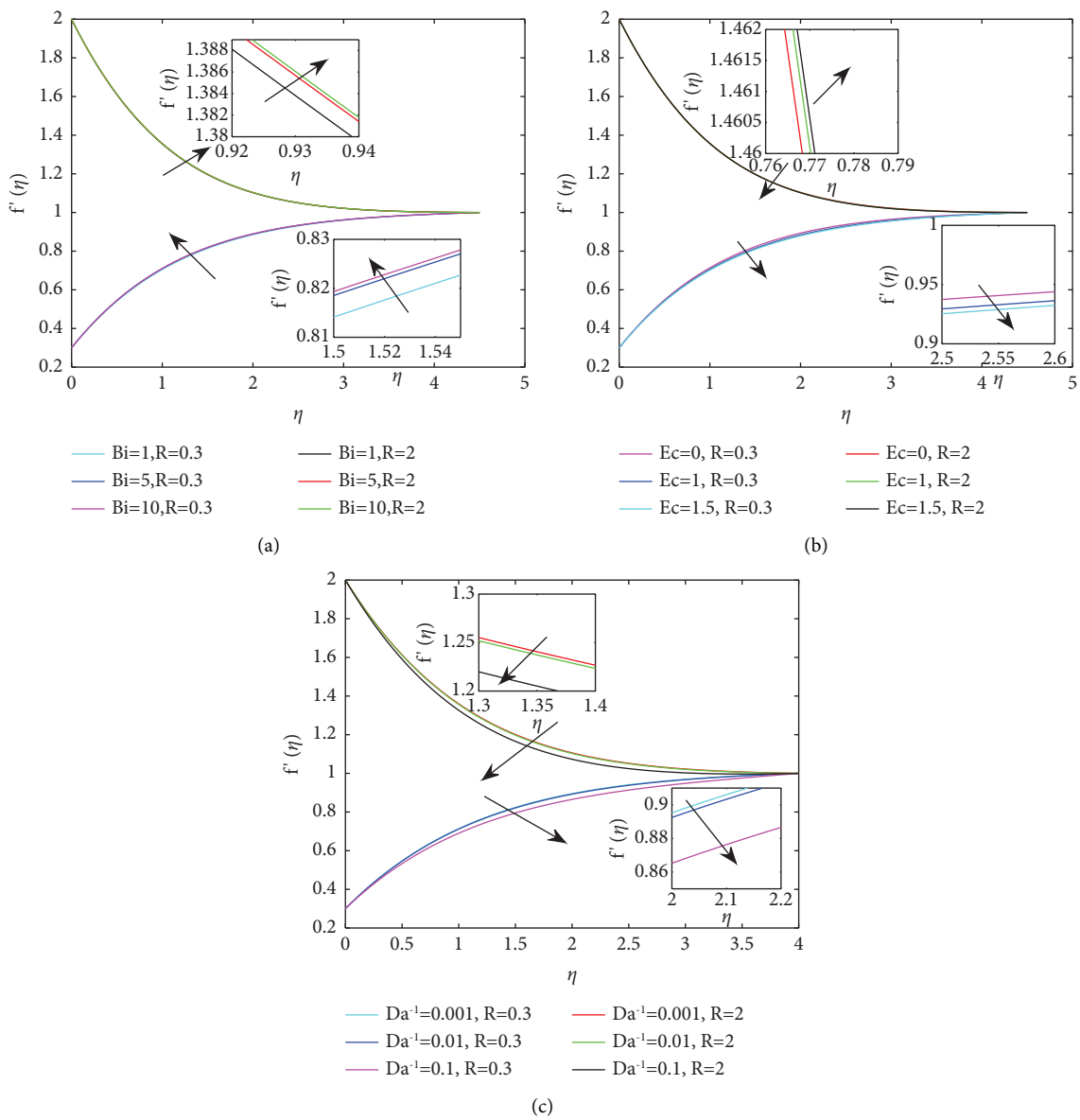

Figure 4: Impacts of Biot number B_i, Eckert number Ec, and Darcy parameter $(\mathrm{Da})^{-1}$ on the velocity profile. (a) $f'(\eta)$ for various values of B_i. (b) $f'(\eta)$ for various values of Ec. (c) $f'(\eta)$ for various values of $(\mathrm{Da})^{-1}$.

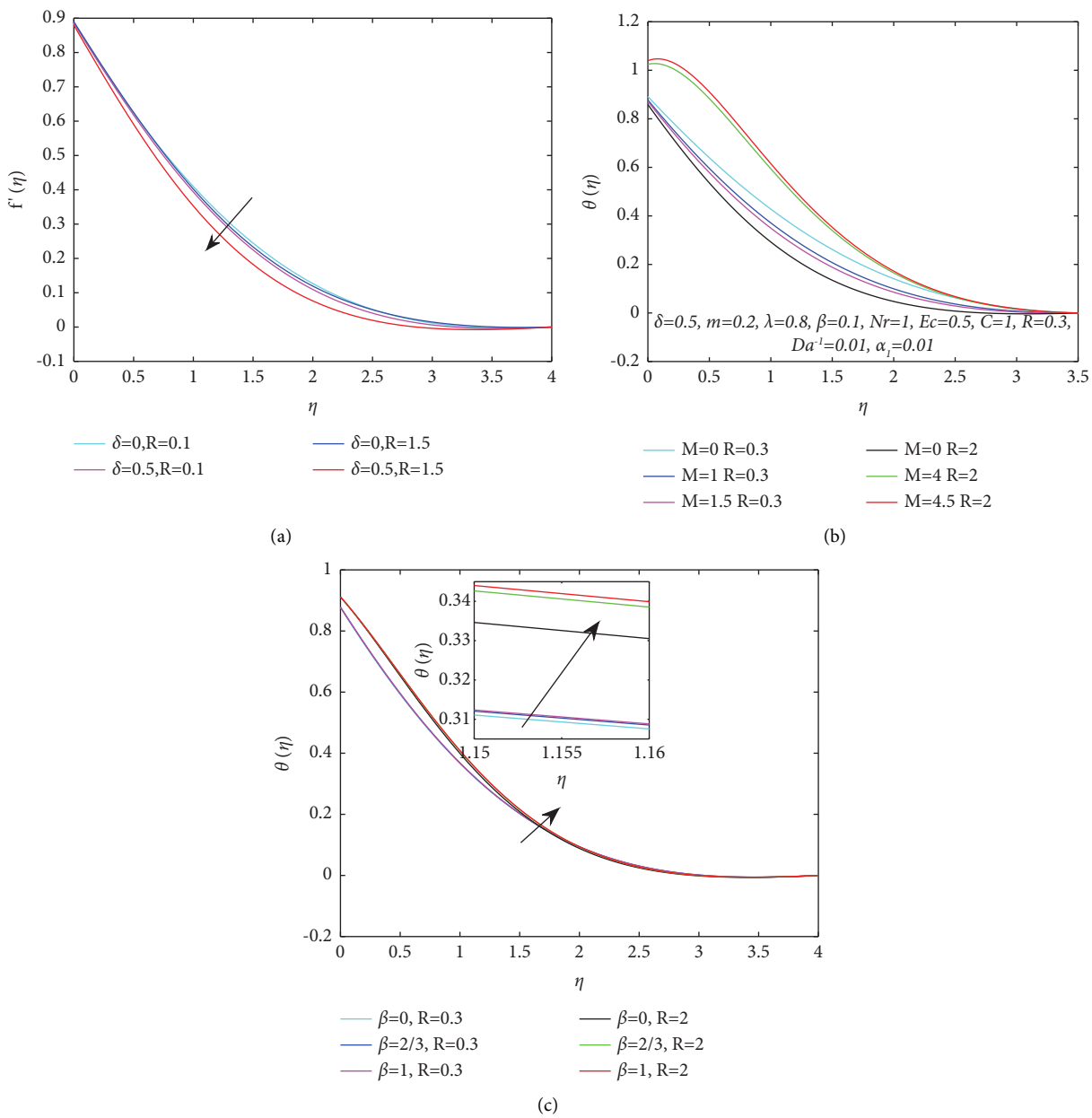

Figure 5: Influence of the Casson parameter δ, magnetic parameter M, and wedge angle β on the temperature profile. (a) $\theta(\eta)$ for various values of δ. (b) $\theta(\eta)$ for various values of M. (c) $\theta(\eta)$ for various values of β.

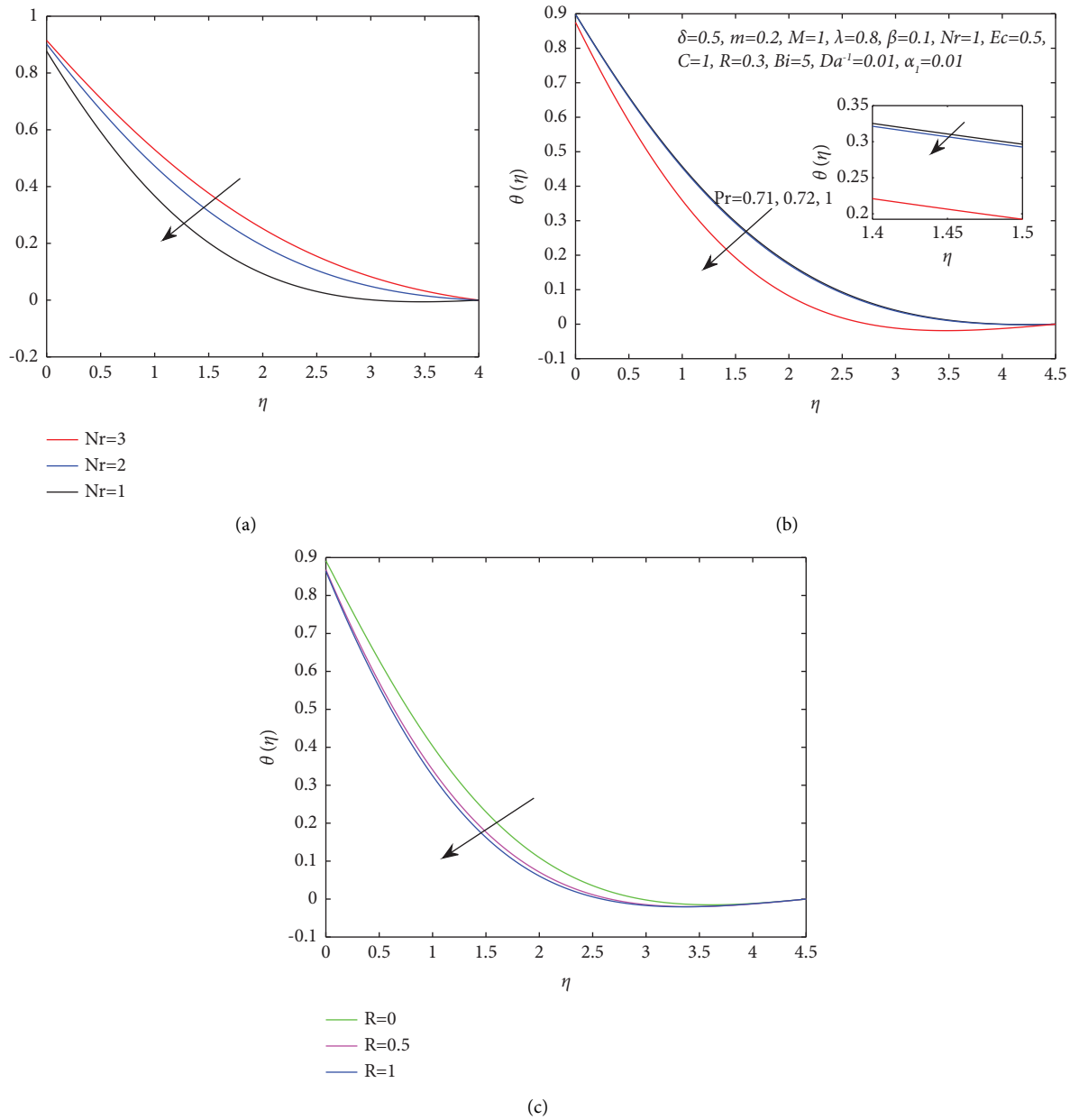

Figure 6: Impacts of the radiative heat transfer parameter Nr, Prandtl number Pr, and velocity ratio parameter R on the temperature profile. (a) Impact of Nr at $\theta(\eta)$. (b) Impact of Pr at $\theta(\eta)$. (c) Impact of R at $\theta(\eta)$.

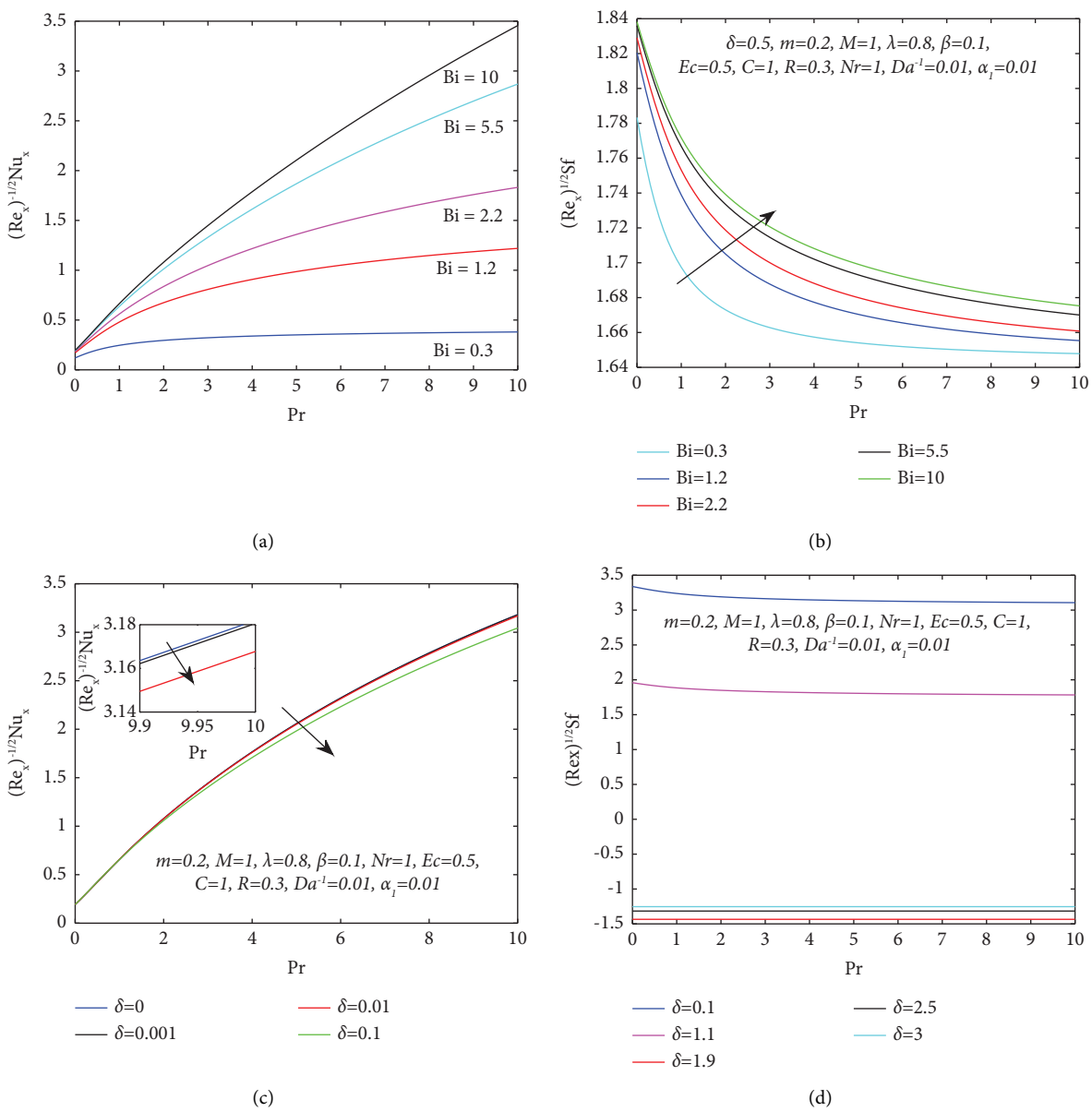

Figure 7: Effects of Biot number B_i and Casson parameter δ on drag force and Nusselt number. (a) Effects of B_i on Nusselt number. (b) Effects of B_i on surface drag force. (c) Effects of δ on Nusselt number. (d) Effects of δ on surface drag force.

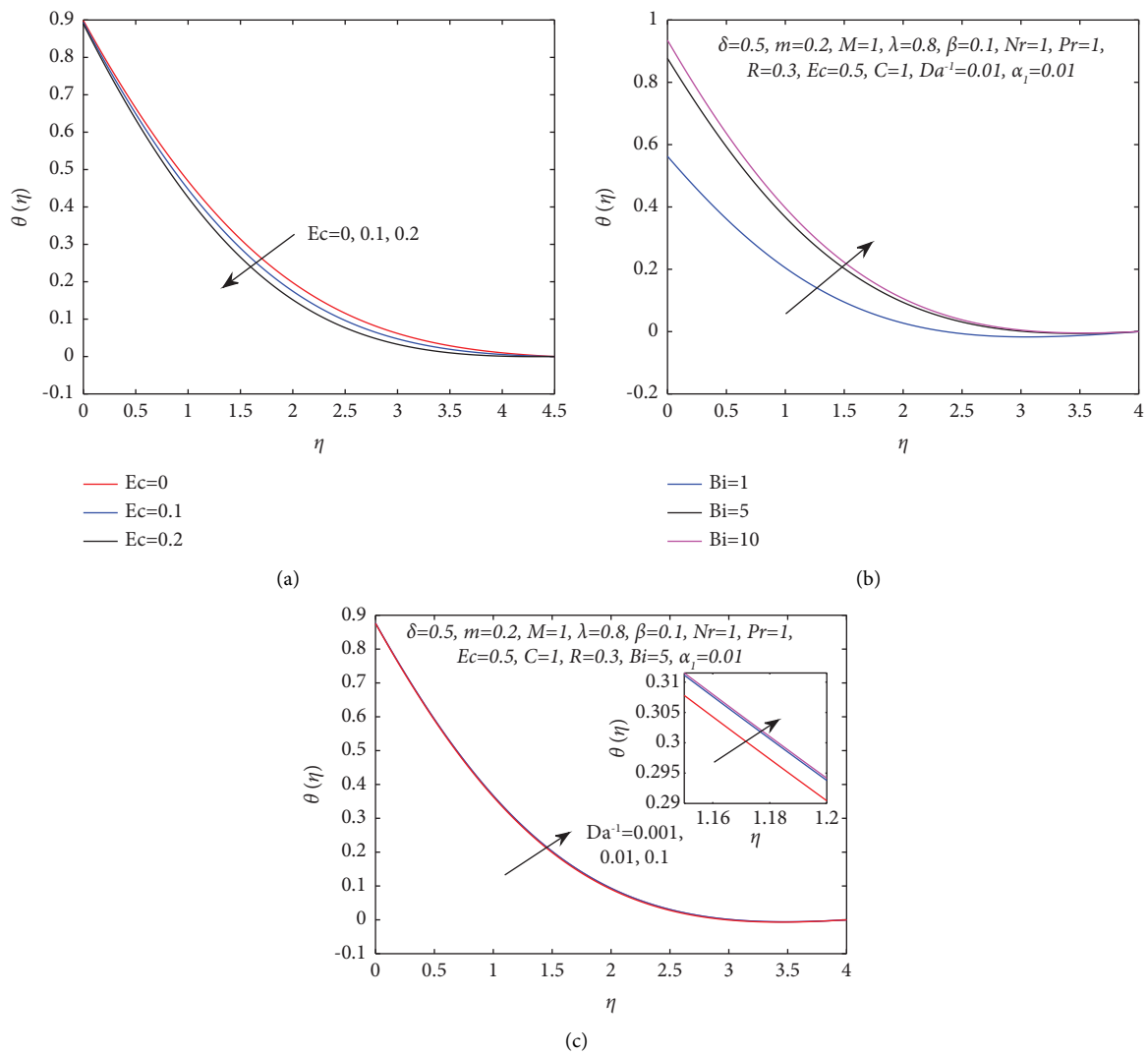

Figure 8: Influence of Eckert number Ec, Biot number B_i, and Darcy parameter $(\mathrm{Da})^{-1}$ on the temperature profile. (a) $\theta(\eta)$ for various values of Ec. (b) $\theta(\eta)$ for various values of B_i. (c) $\theta(\eta)$ for various values of $(\mathrm{Da})^{-1}$.

decreases as Pr increases. The Nusselt number is an increasing function of Pr, as Figure 7(c) illustrates, but for a constant value of Pr, it decreases with decreasing values of the Casson parameter δ. Furthermore, Figure 7(d) shows that skin friction rises with the increasing values of δ for a given value of Pr.

7. Conclusions

This paper considers magnetohydrodynamics thermal flow and boundary layer analysis using Casson fluid over an extending wedge by considering porosity, ohmic heating, convective boundary layer conditions, and viscous dissipation. The mathematical model of the problem is a system of nonlinear PDEs. This system is transformed into a set of ODEs with suitable transformations. The obtained boundary value problem is numerically solved by using the shooting method. Tables and graphs give a detailed picture of the different thermodynamic profiles.

The following observations are of notable significance:

(i) As Casson parameter δ increases when $R = 0.3$, $f'(\eta)$ increases and increase in δ when $R = 2$, reduces the depth of momentum boundary layer.

(ii) When M rises with $R < 1$, $f'(\eta)$ increases and when $R = 2$, $f'(\eta)$ decreases.

(iii) At $R = 0.3$ and $R = 2$, the momentum boundary layer decreases by an increase in Da^{-1}.

(iv) As the velocity ratio parameter R increases, $f'(\eta)$ also increases.

(v) $\theta(\eta)$ increases as δ rises at $R = 0.5$, and $\theta(\eta)$ decreases when $R = 2.1$.

(vi) At $R = 0.3$ and $R = 2$, the thermal boundary's thickness is directly related to the angle parameter β.

(vii) It is also detected that the temperature profile reduces with increasing values of the Eckert number Ec.

With a rise in the Prandtl number Pr, the depth of the thermal boundary layer decreases.

(i) When the value of R rises, $\theta(\eta)$ decreases.

(ii) Decrease in the Darcy number Da increases the temperature profile $\theta(\eta)$.

(iii) Nusselt number and drag force are the increasing functions of Biot number B_i.

(iv) Increasing the Casson parameter enhances the skin friction and reduces the Nusselt number.

The findings of this investigation contribute to problems in fluid dynamics and heat transfer that involve studying the behavior of a non-Newtonian fluid with Casson rheological properties near a solid porous wedge surface. Such problems are common in various engineering and scientific applications, including chemical engineering, biomedical engineering, and materials processing. In biomedical engineering, within the context of blood flow, the Casson parameter considered in this analysis describes the behavior of non-Newtonian blood flow in arteries and veins. In the pharmaceutical industry, the Casson parameter characterizes the rheological properties of pharmaceutical suspensions and emulsions, thus playing a vital role in the formulation and manufacturing of drugs. In polymer suspensions, the Casson parameter is vital in extrusion and injection molding processes. The findings of this investigation and the data obtained through numerical calculations delineate the variational changes in the physical parameters of importance, i.e., the skin-friction coefficient and Nusselt number. Therefore, it is recommended to reinvestigate some related physical problems in the field of applications as mentioned earlier based on the findings of the present investigation.

Nomenclature

(u, v) [ms^{-1}]:	x and y components of velocity
(x, y):	Cartesian coordinates
T [K]:	Temperature
T_f [K]:	Temperature of hot fluid
U [ms^{-1}]:	Velocity far away from wedge
U_w [ms^{-1}]:	Velocity of expanding wedge
v_w [ms^{-1}]:	Suction/injection velocity
B [$M^1T^{-2}I^{-1}$]:	Uniform magnetic field
Ω [−]:	Total angle of the wedge
β [−]:	Wedge's angle
h_f [W/m^2/K]:	Heat transfer coefficient
g [ms^{-2}]:	Gravity field
σ [$M^{-1}L^{-3}T^3A^2$]:	Conductivity of fluid due to electric current
q_r [kWm^{-2}]:	Radiative heat flux
ψ:	Stream function temperature
c_p [$M^oL^2T^{-2}K^{-1}$]:	Specific heat capacity
δ [−]:	Casson parameter
C_b:	Drag coefficient
C_f [−]:	Skin friction
Nu$_x$ [−]:	Nusselt number
M [−]:	Magnetic parameter
λ:	Mixed convective parameter
Gr$_x$ [−]:	Grashof number
Re$_x$ [−]:	Reynold number
Nr:	Radiative heat transfer parameter
Ec:	Eckert number
Pr [−]:	Prandtl number
B_i [−]:	Biot number
R [−]:	Velocity ratio parameter
(Da)$^{-1}$ [−]:	Darcy inverse
α_1 [Kgm^2]:	Local inertia parameter

Greek Symbols

k [Wm$^{-1}K^{-1}$]:	Thermal conductivity
ϕ [−]:	Porosity parameter
β_o [−]:	Thermal expansion parameter
ρ [ML^{-3}]:	Mass density
ν [$M^OL^2T^{-1}$]:	Kinematic viscosity
θ [−]:	Dimensionless temperature.

Data Availability

No data were used to support the findings of this study.

Conflicts of Interest

The authors declare that they have no conflicts of interest.

Authors' Contributions

Dur-e-Shehwar Sagheer conducted conceptualization, methodology, handled software, formal analysis, and writing of the original draft. M. Sabeel Khan and M. Asif Memon performed writing of the original draft, collected resources, data curation, investigation, visualization, and validation. R. Shehzad and Amsalu Fenta conducted project administration, writing of the review, editing, and supervision. Mohammad Alqudah conducted validation, investigation, physical interpretation, writing of the review, and editing. Nawal A. Alshehri has contributed in the final drafting of the revised version of the paper by reviewing it critically for important intellectual content, editing, and proofreading. However, he has also addressed a few points of the revision.

Acknowledgments

The researchers would like to acknowledge the Deanship of Scientific Research, Taif University, Saudi Arabia, for funding this work.

References

[1] N. A. Shah, A. Wakif, B. Mahanthesh, and R. Sivaraj, *Ratio of Momentum Diffusivity to thermal Diffusivity: Introduction, Meta-Analysis, and Scrutinization*, CRC Press, Boca Raton, FL, USA, 2022.

[2] A. Ishak, R. Nazar, and I. Pop, "Mhd mixed convection boundary layer flow towards a stretching vertical surface with constant wall temperature," *International Journal of Heat and Mass Transfer*, vol. 53, no. 23-24, pp. 5330–5334, 2010.

[3] A. Hossain, N. C. Roy, and S. Siddiqa, "Unsteady mixed convection dusty fluid flow past a vertical wedge due to small fluctuation in free stream and surface temperature," *Applied Mathematics and Computation*, vol. 293, pp. 480–492, 2017.

[4] T. Dil and M. S. Khan, "A non-Fourier approach towards the analysis of heat transfer enhancement with water based nanofluids through a channel," *AIP Advances*, vol. 8, no. 5, Article ID 055311, 2018.

[5] M. V. Karwe and Y. Jaluria, *Fluid Flow and Mixed Convection Transport from a Moving Plate in Rolling and Extrusion Processes*, ASME Journal of Heat and Mass Transfer, vol. 110, no. 3, pp. 655–661, 1988.

[6] M. V. Karwe and Y. Jaluria, "Numerical simulation of thermal transport associated with a continuously moving flat sheet in rolling or extrusion," *American Society of Mechanical Engineers, Heat Transfer Division,(Publication) HTD*, vol. 96, p. 37, 1988.

[7] M. K. Nayak, G. C. Dash, and L. P. Singh, "Heat and mass transfer effects on MHD viscoelastic fluid over a stretching sheet through porous medium in presence of chemical reaction," *Propulsion and Power Research*, vol. 5, no. 1, pp. 70–80, 2016.

[8] M. K. Nayak, "Chemical reaction effect on MHD viscoelastic fluid over a stretching sheet through porous medium," *Meccanica*, vol. 51, no. 8, pp. 1699–1711, 2016.

[9] S. Saleem, M. A. Memon, M. S. Khan, and K. Jacob, "Heat transfer through a higher grade forchheimer porous cuo–h2o-nano-medium confined between non-isothermal moving plates," *Case Studies in Thermal Engineering*, vol. 47, pp. 1–19, 2023.

[10] R. Ravindran, S. Roy, and E. Momoniat, "Effects of injection (suction) on a steady mixed convection boundary layer flow over a vertical cone," *International Journal of Numerical Methods for Heat and Fluid Flow*, vol. 19, no. 3/4, pp. 432–444, 2009.

[11] I. Ullah, I. Khan, and S. Shafie, "Hydromagnetic falkner-skan flow of casson fluid past a moving wedge with heat transfer," *Alexandria Engineering Journal*, vol. 55, no. 3, pp. 2139–2148, 2016.

[12] B. K. Sharma, A. Kumar, R. Gandhi, and M. M. Bhatti, "Exponential space and thermal-dependent heat source effects on electro-magneto-hydrodynamic Jeffrey fluid flow over a vertical stretching surface," *International Journal of Modern Physics B*, vol. 36, no. 30, Article ID 2250220, 2022.

[13] J. Chamkha, M. Mujtaba, A. Quadri, and C. Issa, "Thermal radiation effects on mhd forced convection flow adjacent to a non-isothermal wedge in the presence of a heat source or sink," *Heat and Mass Transfer*, vol. 39, no. 4, pp. 305–312, 2003.

[14] M. Anwar Hossain, S. Bhowmick, and R. S. R. Gorla, "Unsteady mixed-convection boundary layer flow along a symmetric wedge with variable surface temperature," *International Journal of Engineering Science*, vol. 44, no. 10, pp. 607–620, 2006.

[15] X. Su, L. Zheng, X. Zhang, and J. Zhang, "Mhd mixed convective heat transfer over a permeable stretching wedge with thermal radiation and ohmic heating," *Chemical Engineering Science*, vol. 78, no. 1–8, pp. 1–8, 2012.

[16] R. Kandasamy, I. Muhaimin, and A. B. Khamis, "Thermophoresis and variable viscosity effects on mhd mixed convective heat and mass transfer past a porous wedge in the presence of chemical reaction," *Heat and Mass Transfer*, vol. 45, no. 6, pp. 703–712, 2009.

[17] K. V. Prasad, P. S. Datti, and K. Vajravelu, "Mhd mixed convection flow over a permeable non-isothermal wedge," *Journal of King Saud University Science*, vol. 25, no. 4, pp. 313–324, 2013.

[18] M. Khan, M. Irfan, L. Ahmad, and W. A. Khan, "Simultaneous investigation of mhd and convective phenomena on time-dependent flow of carreau nanofluid with variable properties: dual solutions," *Physics Letters A*, vol. 382, no. 34, pp. 2334–2342, 2018.

[19] S. M. Khan, M. Hammad, S. Batool, and H. Kaneez, "Investigation of mhd effects and heat transfer for the upper-convected Maxwell (ucm-m) micropolar fluid with joule heating and thermal radiation using a hyperbolic heat flux equation," *The European Physical Journal Plus*, vol. 132, no. 4, pp. 158–217, 2017.

[20] N. K. Mishra, M. Sharma, B. K. Sharma, and U. Khanduri, "Soret and Dufour effects on MHD nanofluid flow of blood through a stenosed artery with variable viscosity," *International Journal of Modern Physics B*, vol. 37, no. 30, Article ID 2350266, 2023.

[21] R. Gandhi, B. K. Sharma, N. K. Mishra, and Q. M. Al-Mdallal, "Computer simulations of EMHD casson nanofluid flow of blood through an irregular stenotic permeable artery: application of koo-kleinstreuer-Li correlations," *Nanomaterials*, vol. 13, no. 4, p. 652, 2023.

[22] B. K. Sharma, R. Gandhi, T. Abbas, and M. M. Bhatti, "Magnetohydrodynamics hemodynamics hybrid nanofluid flow through inclined stenotic artery," *Applied Mathematics and Mechanics*, vol. 44, no. 3, pp. 459–476, 2023.

[23] R. Gandhi and B. K. Sharma, "Modelling pulsatile blood flow using casson fluid model through an overlapping stenotic artery with Au-Cu hybrid nanoparticles: varying viscosity approach," *Advances in Mathematical Modelling, Applied Analysis and Computation*, vol. 666, pp. 155–176, 2023.

[24] R. Gandhi, B. Sharma, Q. M. Al-Mdallal, and H. Mittal, "Entropy generation and shape effects analysis of hybrid nanoparticles (Cu-Al2O3/blood) mediated blood flow through a time-variant multi-stenotic artery," *International Journal of Thermofluids*, vol. 18, Article ID 100336, 2023.

[25] M. K. Nayak, J. Prakash, D. Tripathi, V. S. Pandey, S. Shaw, and O. D. Makinde, "3D Bioconvective multiple slip flow of chemically reactive Casson nanofluid with gyrotactic microorganisms," *Heat Transfer- Asian Research*, vol. 49, no. 1, pp. 135–153, 2020.

[26] M. Nayak, J. Prakash, D. Tripathi, and V. S. Pandey, "3D radiative convective flow of ZnO-SAE50nano-lubricant in presence of varying magnetic field and heterogeneous reactions," *Propulsion and Power Research*, vol. 8, no. 4, pp. 339–350, 2019.

[27] F. Mabood, T. Muhammad, M. K. Shaw, and M. Alghamdi, "Numerical simulation for entropy optimized nonlinear radiative flow of GO-Al2O3 magneto nanomaterials with auto catalysis chemical reaction," *Numerical Methods for Partial Differential Equations*, vol. 38, no. 3, pp. 329–358, 2022.

[28] M. K. Nayak, A. Patra, and A. Misra, "Effects of non-uniform suction, heat generation/absorption and chemical reaction with activation energy on MHD falkner-skan flow of tangent hyperbolic nanofluid over a stretching/shrinking eedge," *Journal of Applied and Computational Mechanics*, vol. 6, no. 3, pp. 640–652, 2020.

[29] W. Cao, A. Il, S. J. Yook, O. Va, and X. Ji, "Simulation of the dynamics of colloidal mixture of water with various nanoparticles at different levels of partial slip: ternary-hybrid nanofluid," *International Communications in Heat and Mass Transfer*, vol. 135, Article ID 106069, 2022.

[30] I. Ullah, S. Shafie, I. Khan, and K. L. Hsiao, "Brownian diffusion and thermophoresis mechanisms in casson fluid over a moving wedge," *Results in Physics*, vol. 9, pp. 183–194, 2018.

[31] S. Bilal, M. Sohail, and R. Naz, "Heat transport in the convective casson fluid flow with homogeneous–heterogeneous reactions in Darcy–forchheimer medium," *Multidiscipline Modeling in Materials and Structures*, vol. 15, no. 6, pp. 1170–1189, 2019.

[32] M. S. Khan and T. Dil, "Heat transfer enhancement of automobile radiator using h2o–cuo nanofluid," *AIP Advances*, vol. 7, no. 4, Article ID 045018, 2017.

[33] I. H. Qureshi, J. Alebraheem, M. B. Hafeez, M. S. Khan, and A. Elmoasry, "Particle rotation effects in cosserat-maxwell boundary layer flow with non-fourier heat transfer using a new novel approach," *Scientia Iranica*, vol. 28, no. 3, pp. 1223–1235, 2021.

[34] M. S. Khan and H. Kaneezl, "Numerical computation of heat transfer enhancement through cosserat hybrid nanofluids using continuous galerkin–petrov method," *The European Physical Journal Plus*, vol. 135, pp. 1–18, 2020.

[35] M. Hussain, A. Ghaffar, A. Ali et al., "Mhd thermal boundary layer flow of a casson fluid over a penetrable stretching wedge in the existence of nonlinear radiation and convective boundary condition," *Alexandria Engineering Journal*, vol. 60, no. 6, pp. 5473–5483, 2021.

[36] J. Buongiorno, *Convective Transport in Nanofluids*, ASME Journal of Heat and Mass Transfer, vol. 128, no. 3, pp 240–250, 2006.

[37] S. Mukhopadhyay, K. Bhattacharyya, and T. Hayat, "Exact solutions for the flow of casson fluid over a stretching surface with transpiration and heat transfer effects," *Chinese Physics B*, vol. 22, no. 11, Article ID 114701, 2013.

[38] M. Hussain, W. Khan, U. Farooq, and R. Razzaq, "Impact of non-similar modeling for thermal transport analysis of mixed convective flows of nanofluids over vertically permeable surface," *Journal of Nanofluids*, vol. 12, no. 4, pp. 1074–1081, 2023.

[39] A. Jan, M. Mushtaq, U. Farooq, and M. Hussain, "Nonsimilar analysis of magnetized Sisko nanofluid flow subjected to heat generation/absorption and viscous dissipation," *Journal of Magnetism and Magnetic Materials*, vol. 564, Article ID 170153, 2022.

[40] J. Cui, A. Jan, U. Farooq, M. Hussain, and W. A. Khan, "Thermal analysis of radiative Darcy–forchheimer nanofluid flow across an inclined stretching surface," *Nanomaterials*, vol. 12, no. 23, p. 4291, 2022.

[41] U. Farooq, M. E. A. Rabie, M. Hussain, J. Cui, and T. Muhammad, "Nonsimilar modeling and numerical simulations of electromagnetic radiative flow of nanofluid with entropy generation, mathematical problems in engineering," *Journal of Nanofluids*, vol. 2022, Article ID 4272566, 2022.

[42] L. F. Shampine and J. Kierzenka, "A BVP Solver based on residual control and the MATLAB PSE," *ACM Transactions on Mathematical Software*, vol. 27, no. 3, pp. 3299–3161, 2001.